PCCP

Accepted Manuscript

ROYAL SOCIETY OF CHEMISTRY

www.rsc.org/pccp

Ab initio Molecular Dynamics Simulations of Aqueous Triflic Acid Confined in Carbon Nanotubes

Jeffrey K. Clark II,[†] Bradley F. Habenicht,[‡] and Stephen J. Paddison[†,*]

[†]*Department of Chemical and Biomolecular Engineering, University of Tennessee, Knoxville, TN 37996*
[‡]*School of Natural Sciences, University of California, Merced, CA 95343*

ABSTRACT

Ab initio molecular dynamics simulations were performed to investigate the effects of nanoscale confinement on the structural and dynamical properties of aqueous triflic acid (CF_3SO_3H). Single-walled carbon nanotubes (CNTs) with diameters ranging from ~11 to 14 Å were used as confinement vessels, and the inner surface of the CNT were either left bare or fluorinated to probe the influence of the confined environment on structural and dynamical properties of the water and triflic acidic. The systems were simulated at hydration levels of n = 1 – 3 H_2O/CF_3SO_3H. Proton dissociation expectedly increased with increasing hydration. Along with the level of hydration, hydrogen bond connectivity between the triflic acid molecules, both directly and via a single water molecule, played a role on proton dissociation. Direct hydrogen bonding between the CF_3SO_3H molecules, most commonly found in the larger bare CNT, also promoted interactions between water molecules allowing for greater separation of the dissociated protons from the $CF_3SO_3^-$ as the hydration level was increased. However, this also resulted in a decrease in the overall proportion of dissociated protons. The confinement dimensions altered both the hydrogen bond network and the distribution of water molecules where the H_2O in the fluorinated CNTs tended to form small clusters with less proton dissociation at n = 1 and 2 but the highest at n = 3. In the absence of nearby hydrogen bond accepting sites from H_2O or triflic acid SO_3H groups, the water molecules formed weak hydrogen bonds with the fluorine atoms. In the bare CNT systems, these involved the CF_3 groups of triflic acid and were more frequently observed when direct hydrogen bonding between CF_3SO_3H hindered potential hydrogen bonding sites. In the fluorinated tubes, interactions with the covalently bound fluorine atoms of the CNT wall dominated which appear to stabilize the hydrogen bond network. Increasing the hydration level increased the frequency of the OH···F (CNT) hydrogen bonding which was highly pronounced in the smaller fluorinated CNT indicating an influence on the confinement dimensions on these interactions.

Keywords: ab initio molecular dynamics, confinement, triflic acid, proton transfer, fuel cell

Corresponding Author

*E-mail: spaddison@utk.edu.

Introduction

Proton exchange membrane fuel cells (PEMFCs) are clean, efficient energy conversion devices that offer potential use for stationary, portable, and automotive power.[1-3] At the heart of PEMFCs is the proton-conducting polymer electrolyte, or proton exchange, membrane (PEM). The wide variety of applications for PEMFCs places demands on the membrane beyond high proton conductivity (≥ 10^{-1} Scm^{-1}) including long-term mechanical durability and high thermal and chemical stability in an oxidative environment at temperatures up to 120°C.[4-7] There are several membrane materials available that meet many of these requirements, but nearly all currently available PEMs are limited by the necessity to be highly hydrated (~95% relative humidity) to sufficiently conduct protons.[6, 8, 9] These conditions result in adverse water 'cross-over' due to electroosmotic drag and permeation and also limit the operating conditions to below 100°C (i.e., the boiling point of water) to prevent drying of the membrane.[10-12] Low temperature operation requires the use of expensive platinum or platinum-based electrocatalysts due to poor electrode reaction kinetics which are also more susceptible to poisoning from trace amounts of carbon monoxide in the hydrogen feed stream blocking the reaction sites at temperatures below 120°C degrading the fuel cell performance.[4]

The most commonly employed PEMs are perfluorosulfonic acid (PFSA) ionomers with Nafion® currently representing the industry standard. PFSA ionomers consist of a hydrophobic poly(tetrafluoroethylene) (PTFE) backbone functionalized with pendant perfluoroether side chains each terminated with a single hydrophilic sulfonic acid group. When these materials are hydrated, phase separation into hydrophilic and hydrophobic domains occurs.[11, 13] Within the aqueous domain the dissociated protons may transfer via vehicular or structural (i.e., 'Grotthuss' type) diffusion.[14-18] In bulk water, protons exist as solvated 'fluxional complexes' with Eigen ($H_9O_4^+$) and Zundel ($H_5O_2^+$) cations as idealized limiting forms,[19, 20] and proton 'shuttling' involves continuous inter-conversions between these limiting forms through transfer reactions driven by dynamical changes in the hydrogen bond network in the second and third hydration shells.[19-25] Nanoscale confinement adds additional complexity to the mechanism of proton transfer in water as the restricted environment can influence the solvation structure of the proton and the hydrogen bond network and dynamics.[26-31] The hydrophilic domains in hydrated PFSA

membranes, containing the water molecules, protons, and acidic groups, are only a few nanometres in diameter which is influenced by the amount of absorbed water and specific ionomer chemistry.[32-37] Proton transport is further complicated by the heterogeneous nature of the ionomer and the presence of acidic groups,[32] and elucidation of the exact nature of proton transport in PEMs is limited by an incomplete molecular-level understanding of their hydrated morphology.[4, 11, 38-41] Nevertheless, it is accepted that, along with the level of hydration and density of acidic groups, proton transport is intimately connected to the formation and breaking of hydrogen bonds which is difficult to resolve experimentally and multiscale modelling techniques are frequently used to probe membrane characteristics at a variety of length and time scales.[4, 42]

Insight into the effects of equivalent weight, molecular weight, and degree of hydration (i.e., H_2Os/SO_3H) on the phase separated morphology has been studied using dissipative particle dynamics (DPD) simulations.[40, 43-45] Several classical molecular dynamics (MD) simulations on hydrated PEMs have also been performed to study hydration and transport properties in systems containing thousands of atoms.[46-50] However, these simulations assume that all acidic protons are dissociated and exist as hydronium (H_3O^+) ions and cannot capture the proton hopping behaviour associated with structural diffusion. Empirical valence bond (EVB) schemes[51-54] capable of incorporating proton shuttling into classical simulations have also been used to effectively simulate proton solvation and transport in PEMs[18, 53, 55-59] but are somewhat limited in their molecular description of proton diffusion at very low levels of hydration ($\lambda \leq 3$).[60] *Ab initio* methods, which allow for the breaking and forming of covalent bonds, have also been used to study proton solvation and transfer in PEMs without the requirement of empirical parameterization or predefined states of the protons but are limited to relatively small system sizes. Static electronic structure calculations on isolated side chain fragments of PFSAs and other PEMs have shown that proton dissociation may not occur at hydration levels where $\lambda < 3$.[61-74] However, incorporating multiple side chains revealed that interactions between acidic groups through either direct hydrogen bonds or via a hydrogen bond bridge through a single water molecule or hydronium ion can enhance proton dissociation at low hydration levels.[75-80] Dynamical information can be obtained through *ab initio* molecular dynamics

(AIMD) simulations, though the membranes are too complex to be fully treated with these techniques, and model systems are typically employed.[81-92]

Our previous AIMD simulations utilized carbon nanotubes (CNTs) functionalized with $-CF_2SO_3H$ groups to explore the factors that contribute to proton dynamics in PFSA ionomers a simplified confined environment.[84-86] Although the model systems are much more homogenous than true PFSA membranes, the use of CNTs provides a framework that allows for alteration of relevant parameters that may influence proton dissociation and transport such as channel size and environment, spacing of acid groups, and degree of hydration. Nanotubes with three different diameters (11.2, 13.2, and 14.1 Å) were chosen to explore the effects of the confinement dimensions, and the nanotube walls were either left bare or fluorinated to study the influence the hydrophobicity of the confined surface has on transport properties. The simulations were conducted at hydration levels of $\lambda = 1$ and 3. Systems with less separation between sulfonic acid groups resulted in increased proton dissociation but also increased the formation of trap states where a dissociated proton exists as a hydronium ion bridging two sulfonic acid groups hindering long-range proton transport. The fluorinated nanotube walls were found to provide sites that could accept weak hydrogen bonds from the water molecules which stabilized the hydrogen bond network and increased the observed proton dissociation. This is consistent with results of IR spectroscopy studies on Nafion which showed evidence that absorbed water potentially interacts with the hydrophobic fluorocarbon backbone.[93-95] Evidence of weak hydrogen bond-like interactions was also found in AIMD simulations on hydrates of trifluoromethanesulfonic acid (triflic acid): $CF_3SO_3H(H_2O)_n$ where n = 1,2,4, and 5.[87, 88] This was found to occur when a water molecule accepted a hydrogen bond from a triflic acid SO_3H group with a CF_3 group in the near vicinity in the absence of any other water molecules or triflic acid oxygen atoms to hydrogen bond with. Limited water was also determined to increase the formation of defect structures that included two triflic acid sulfonate groups sharing a single proton and proton transfer to a single water molecule that bridge multiple sulfonate groups. Furthermore, inclusion of quantum nuclear effects via path integral techniques was found to delocalize the proton defect which increased the Zundel character of the defect structure in each of the hydrates.[87]

Here, we present the results of an extension of our previous work[84-86] using AIMD to investigate the behaviour of mobile triflic acid and water confined in single-walled CNTs of various diameters water content of n = 1 – 3 H_2O/CF_3SO_3H. The impact of the nature of the confined environment on structural properties is investigated through functionalizing the nanotube walls with fluorine atoms. This paper is organized as follows. The systems and computational methodology are first described. This is followed by presentation and discussion of the results which include hydrogen bonding and coordination numbers, connectivity of the hydrogen bond network, proton dissociation and radial distribution functions, and interactions between the water molecules and fluorine atoms. Finally, important results are summarized in the conclusions section.

Computational Methods

Ab initio molecular dynamics simulations were performed using the Vienna *Ab Initio* Simulation Package (VASP).[96-99] Core electrons were treated using the projector-augmented-wave (PAW) method.[100, 101] The Perdew–Burke–Ernzerhof (PBE) generalized gradient approximation for the exchange-correlation functional was used,[102, 103] and the electronic subsystem was sampled at the Γ-point of the first Brillouin zone with a plane wave cutoff of 400 eV and a Gaussian smearing of 0.03 eV. The calculations are spin unpolarised. CNTs with chirality (14,0) and (17,0) were chosen as encapsulation vessels for the water molecules and triflic acid. The inner walls of the CNTs were either left bare or fluorinated to model different hydrophobic environments. The fluorine atoms were added to every next nearest neighbour carbon atom as uniformly as possible. All of the systems were simulated at water contents of n = 1 – 3 H_2O/CF_3SO_3H. The total density of triflic acid and water within the CNTs was, as close as possible, the same for all systems. This was maintained by either using nanotubes of different lengths or slightly varying the CNT carbon–carbon bond length. As addition of fluorine atoms to the CNT wall effectively reduced the accessible volume, fewer triflic acid molecules were added in the fluorinated systems. Some relevant system parameters are given in Table 1. The nomenclature used to distinguish between the different CNT systems closely follows that of the previous work:[84-86] 14 and 17 are used for the different CNT chirality followed by ‘F’ or ‘N’ for fluorinated and nonfluorinated, and 1, 2, or 3 to designate the hydration level. For example, the (14,0)

CNT system with fluorinated walls at a water content of n = 2 would read 14F2. Representative images of the systems are shown in Figure 1. As with the previous studies,[84-86] the carbon atoms of the CNT wall and the attached fluorine atoms (when applicable) were held fixed, and periodic boundary conditions were imposed with 4 Å of vacuum added in the perpendicular directions to avoid interactions with other images in the supercell. The systems were initially relaxed to their minimum energy configuration and then annealed to 600 K via repeated velocity rescaling and then returned back down to 300 K. This was followed by 3 ps simulations in the canonical ensemble and 3 ps of microcanonical MD for equilibration which were discarded. Born–Oppenheimer AIMD trajectories of up to 30 ps were generated with a time step of 0.5 fs in the microcanonical ensemble for data analysis. We note that the PBE functional does not account for dispersion interactions or include exact exchange. The simulations were performed using VASP 4.6 which does not include hybrid or dispersion corrected functionals. However, we were able to obtain test geometry relaxations using VASP 3.5.3 on a representative configuration of the 14N3 system using PBE0,[104] HSEsol,[105] PBE-D3,[106] and vdW-optB86b[107, 108] and for 17F3 with PBE-D3[106] and vdW-optB86b[107, 108] to test the sensitivity of the hydrogen bond structure using hybrid and dispersion corrected functionals. The results are reported in Tables S1 and S2 for 14N3 and 17F3, respectively, and reveal only slight differences obtained using the different functionals. We were also able to obtain a short MD sample on 14N3 using VASP 5.2.11 with PBE-D2[109] to include empirical dispersion corrections. The overall structure and average hydrogen bond distances were essentially identical using both PBE and PBE-D2. This was also the case for the proton dissociation data given in Table S3. Furthermore, inclusion of dispersion and exact exchange has also been shown to be minimal on the structure of and proton transfer in water confined in CNTs using AIMD with the PBE functional.[30] We, thus, believe that the impact of these effects on the predicted results would be minimal.

Results and Discussion

Hydrogen bonding and coordination numbers

Several of the analyses that follow regard hydrogen bonding between the water molecules and triflic acid molecules. In this study, a hydrogen bond was taken to exist if the oxygen–

oxygen separation was less than 3.25 Å with an H–O···O angle less than 30°.[110, 111] The coordination numbers (CN) for the water molecules is defined as the average number of donating and accepting hydrogen bonds per water molecule. Figure 2 shows the average water CN based on H_2O/H_2O hydrogen bonds, H_2O/CF_3SO_3H hydrogen bonds, and the total CN for each of the systems. It should be noted that at this stage, we refer to the CNs regarding water molecules and the triflic acid SO_3H groups for ease of discussion, but these also, respectively, encompass hydrogen bonds involving Zundel and hydronium ions and triflate ($CF_3SO_3^-$) anions and will not be distinguished unless necessary. Representative snapshots of the hydrogen bonding in each system for n = 1, 2, and 3 are shown in Figures 3, 4, and 5, respectively. At n = 1, the average total H_2O CN is approximately 2 in all cases but result from different contributions from H_2O/H_2O and H_2O/CF_3SO_3H hydrogen bonds in the different systems. In the bare nanotubes, which have a slightly higher total CN, hydrogen bonding between water molecules occurs while in the fluorinated CNTs the water molecules are isolated from each other. Typical configurations in the fluorinated systems involve a water molecule donating a hydrogen bond to a CF_3SO_3H and accepting a hydrogen bond from an adjacent one with no direct interactions between the acid molecules. In the smaller CNT, this is in the form of a highly aligned hydrogen bond wire (Figure 3b) while in the larger system the pattern is less uniform. Hydrogen bonding between triflic acid molecules in the bare systems occurs regularly which promotes interactions between the water molecules at this low water content. An increase in the number of hydrogen bonds between water molecules was observed in all systems upon increasing the hydration to n = 2. The total CN also increases in all cases except 14F2 which is approximately the same as that of the lower hydration level. The typical structure in this case exhibits somewhat selective solvation of a single CF_3SO_3H by three water molecules with the other CF_3SO_3H oriented parallel to the CNT axis only involved in one hydrogen bond with a single water molecule (Figure 4b). The average total H_2O CNs in the bare systems are each ~2.5. In the smaller CNT, the contributions are essentially split between hydrogen bonds to and from water and triflic acid molecules. A greater proportion of hydrogen bonds in the larger tube occur between water molecules with slightly less than 1 hydrogen bond per water molecule to or from a CF_3SO_3H, on average, and generally one direct hydrogen bond between triflic acid molecules. The total CN in 17F2 of ~2.25 is

slightly less than 17N2, but with nearly the same CN between water molecules. The typical hydrogen bond structure contains one direct hydrogen bond between triflic acid molecules with the H_2O hydrogen bonding among themselves as well as bridging the other triflic acid oxygen atoms through two or more water molecules. At n = 3, the average H_2O–CF_3SO_3H CNs for the smaller CNTs is ~1. In 14F3, this is a result of configurations where each H_2O donates one hydrogen bond to a triflic acid molecule. In 14N3, on the other hand, this arises due to typical configurations containing two or three water molecules not hydrogen bonded to any triflic acid SO_3H groups but multiple different water molecules involved in direct hydrogen bonds to two different CF_3SO_3H effectively bridging the triflic acid molecules. In 17F3, bridging of two triflic acid molecules through one H_2O occurred frequently as well as one triflate oxygen atom accepting hydrogen bonds from two different water molecules. It was not common to find water molecules isolated from the triflic acid molecules which results in the highest H_2O–CF_3SO_3H CN of all systems at this hydration level. The highest H_2O–H_2O CN and lowest H_2O–CF_3SO_3H CN at n = 3 were found in 17N3. This indicates that the water molecules are more clustered together with rare occurrence of a water molecule involved in hydrogen bonds with multiple triflic acid SO_3H groups. At all water contents, the larger bare CNT contained strong direct hydrogen bonds between triflic acid molecules with short O···O separations that hindered accessibility of water molecules to these sites.

Hydrogen bond connectivity

Along with local hydrogen bonding between neighbouring water and triflic acid molecules, the hydrogen bond network connectivity throughout the entire system is important to proton dissociation and transfer in PEMs.[32] To analyse the connectivity, a similar, but not identical, procedure of previous studies was employed.[85-88, 112, 113] An undirected graph with oxygen atoms as nodes and hydrogen bonds involving two oxygen atoms as edges was used to generate an N x N adjacency matrix, A, at each time step (where N is the total number of oxygen atoms). If a hydrogen bond existed between oxygen atoms i and j, the corresponding matrix elements A_{ij} and A_{ji} were set to 1, otherwise the matrix elements were set to 0. This differs from some of the previous studies where a directed graph was used to obtain the adjacency matrix with elements equal to 1 for hydrogen bonds donated from i and accepted by j (i.e., $A_{ij} \neq A_{ji}$). In these studies the property of

adjacency matrices that element $A_{ij}^{(m)}$ of A^m gives the number of unique walks with m edges from node i to node j. Although the directionality of hydrogen bonds plays an important role in long range proton transport,[114] the aim here is to gain additional insight into the overall hydrogen bond network structure. If a directed graph was used to map the adjacency matrix in the present study, hydronium ions, which rarely accept hydrogen bonds in these simulations, can terminate a path and defining the donor and acceptor in perfectly symmetric sharing of a proton between oxygen atoms is ambiguous. Additionally, the powers of the adjacency matrix using an undirected graph result in unwanted direct revisiting of edges leading to fictitiously long chains. Hence, a slightly difference approach is used here. A simple depth-first search algorithm was used to determine the connectivity matrix, C, whose elements C_{ij} and C_{ji} are 1 if a path of any length connected atoms i and j and 0 otherwise. This allowed for the decomposition of the entire hydrogen bond network into isolated subnetworks. Within each subnetwork a recursive branching algorithm was used to calculate the length (determined by the number of oxygen atoms) of all the chains longer than 2 that did not include a complete ring, though individual oxygen atoms that were part of a ring were initially allowed. The longest chain from each subnetwork was extracted for analysis (i.e., no chains that were branches off of the longest chain were included). All rings that did not include smaller rings were included. Further analysis was performed when rings were present by setting all elements of A_{ij} that were part of a ring to 0 and repeating the process to separate networks of rings and chains. The connectivity results are presented in Table 2 and Figures 6, 7, and 8. Snapshots of rings in systems where ring formation occurred at least 10% of the time are shown in Figures S1 and S2.

Figure 6 shows the average number of chains in each system with and without the inclusion of ring connections normalized by the number of triflic acid molecules. The rationale behind the normalization becomes evident when comparing the data at n = 1. As previously mentioned, the water molecules in the fluorinated systems at this hydration level are isolated from each other and generally form a hydrogen bond bridge between two CF_3SO_3H. The average number of chains is then dependent on and approximately determined by the number of triflic acid molecules (2 for 14F1 and 3 for 17F1). Thus, the normalization allows for a more direct comparison between systems showing

approximately one chain per CF_3SO_3H in each fluorinated CNT which indicates isolated hydrogen bond networks (note that small values here indicate increased connectivity throughout the system). In the bare CNTs, the water molecules are not isolated and multiple triflic acid molecules can be bridged through multiple H_2O. This is also reflected in the average chain lengths shown in Figure 7 where the average number of water molecules in the chains is greater in the bare CNTs than in the fluorinated tubes. While the maximum length of a chain that can be formed is limited by the number of triflic acid and water molecules, the data shown for the chain length has not been normalized by the number of CF_3SO_3H for convenience of discussion and is partitioned into the type of oxygen atoms involved in the chain. The fraction of total oxygen atoms in the system per chain is also shown as a frame of reference. When the longest chain within a subnetwork terminated in a branch to both a triflic acid and water oxygen atom (i.e., two chains with the same length but different terminating oxygen atoms) the contribution from these particular oxygen atoms to the length of the chain was divided evenly to avoid bias in the results. As no rings were observed in the fluorinated systems and were exceedingly rare in the bare tubes at this level of hydration, the results are not affected by omitting ring connections.

The average length of the chains in each system, as well as the contribution from oxygen atoms from water molecules, generally increases with increasing hydration as expected. The number of chains, however, shows less of an obvious trend. At n = 2 and 3, the number of chains per CF_3SO_3H in the smaller fluorinated tube remains equal to one indicating that the water molecules are still in separated clusters (Figures 4b and 5b) while a slight decrease in value was observed in the smaller bare tube due to increased connectivity throughout the system. Negligible ring formation was found in either of the smaller CNTs at n = 2. However, at n = 3, rings were frequently found in 14N3 with an average of 0.53 rings in the system, as shown in Figure 8a. Note that the average number of rings is not normalized because typically only one ring was present at a time in each system, with a few exceptions, so this number also gives a very close approximation to the fraction of time ring formation was observed. Omitting ring connections in 14N3 resulted in a slight drop in the number of chains and a considerable drop in the average chain length to approximately the value found at n = 2 which contains the same number of triflic acid molecules but fewer H_2O. The ring generally had the same form when present in the simulation which contained

one triflate oxygen atom accepting two hydrogen bonds: one from a hydronium ion that also hydrogen bonded to a different CF_3SO_3H and the other from a neighbouring species that regularly transitioned between H_2O, H_3O^+, and $H_5O_2^+$ states (Figure S2a). Ring formation was found in each of the larger CNT systems at both n = 2 and 3 which also involved a single triflate oxygen atom receiving two hydrogen bonds from different water molecules. As previously mentioned, each of the larger systems at n = 2 contain a direct hydrogen bond between triflic acid molecules, which appears to promote ring formation at this water content. The hydrogen bonding in 17F2 has the water molecules clustered between the triflic acid molecules bridging the two together (Figure 4d) resulting in only one chain (0.5 per CF_3SO_3H in every step) when ring connections are allowed. However, the cluster forms a ring throughout approximately 26% of the trajectory, and with this hydrogen bond topography and minimal water, chains and rings do not independently exist simultaneously (Figure S1b). As such, when the oxygen atoms involved in rings are removed from the analysis, the average number of chains decreases accordingly to ~0.74 (0.34 per CF_3SO_3H) but the average chain length is negligibly impacted. The opposite was found for 17N2, which had the fewest chains per CF_3SO_3H of all systems at all hydration levels with a highly connected hydrogen bond network containing several triflate oxygen atoms accepting multiple hydrogen bonds when rings were present. Similar to 14N3, the removal of ring connections disrupts overall connectivity of the longest chain throughout the system, but the high degree of branching in the hydrogen bond network leads to only a slight decrease in the average number of chains but with shorter lengths (Figure S1a).

The hydrogen bond networks in the larger tubes at n = 3 are well connected with fairly long chains encompassing approximately 50 and 69% of all the oxygen atoms per chain in 17F3 and 17N3, respectively, when ring connections were included. However, rings are, again, fairly common and distinctly different ring structures were commonly found in both systems. The majority of the rings in 17N3 contained one triflate oxygen atom and three or four H_2O/H_3O^+ (Figure S2b top) with two such rings occurring at the same time in ~3% of the simulation. However, in roughly 10% of the simulation rings with lengths of 9 or 10 oxygen atoms were observed that that encompassed nearly all of the water molecules (Figure S2b bottom). This led to the increase in average ring length and decrease in average number of chains when ring connections were removed while the smaller five-membered

rings were responsible for the decrease in the average length of chains as with 17N2. There was less variability in the size of rings formed in 17F3 where 80% of the rings contained one triflate oxygen atom and three water molecules while the other 20% had two oxygen atoms of the same $CF_3SO_3^-$ accepting two hydrogen bonds surrounded by three H_2O/H_3O^+ on each side (Figure S2c) giving an average ring size of 4.8 oxygen atoms. The same reasoning for decreases in the number of chains and the length of chains as 17N3 when ring connections are removed can be applied to 17F3. Interestingly, the high hydrogen bond connectivity in the larger fluorinated tube occurred even though the water molecules were found in separate clusters between triflic acid/triflate molecules. Throughout the trajectory the water and triflic acid molecules were ordered in a regular fashion in what appears to be a domain mostly separated from the triflic acid CF_3 groups, shown in Figure 9, which was not observed in any other system at this hydration level. Unlike 14F3, which contained isolated water clusters that mostly formed hydrogen bonds with the triflic acid sulfonate groups from the side, water molecules in the larger fluorinated CNT were able to form hydrogen bonds from both the sides and below the triflic acid sulfonate groups due to the increased space which leads to a more uniform solvation structure. Although the overall connectivity is high, the water molecules in the clusters separated by the triflate anions in 17F3 do not interact while those in 17N3 form a well-connected channel which may impact long-range proton transfer at this hydration level.

Proton dissociation

Proton dissociation in hydrated PEMs is also known to depend on the water content. In our analysis we define five different states for the acidic protons based on the 'most active hydrogen bond' associated with each site. All protons were first assigned to their nearest neighbour oxygen atom, and the oxygen sites with either one or three nearest neighbour hydrogen atoms were located. The values of the asymmetric stretch coordinate, $\delta = R_{O_aH} - R_{O_dH}$, were then determined for each hydrogen bond associated with the oxygen atom, where R_{O_aH} and R_{O_dH} are the distances from a given hydrogen atom to the acceptor and donor oxygen atoms in the hydrogen bond, respectively. If the nearest neighbour oxygen atom was from a triflic acid molecule, it was considered in the analysis; otherwise, the hydrogen bond with the smallest δ was used to determine the state of the proton. A

proton was said to be bound if its nearest neighbour was an oxygen atom of a triflic acid molecule with $\delta \geq 0.2$ Å. If any pair had $\delta < 0.2$ Å, it was assigned one of three shared states according to the types of the oxygen atoms involved: CF_3SO_3H/CF_3SO_3H shared, CF_3SO_3H/H_2O shared, or H_2O/H_2O shared (i.e., a Zundel cation). It should be noted that the shared states between triflic acid molecules also includes sharing between triflic acid and triflate molecules, which is more commonly observed. Lastly, a hydronium (H_3O^+) state was assigned when a non-triflic acid oxygen atom had three proton neighbours with the smallest $\delta \geq 0.2$ Å. The results of the analysis for each system at all hydration levels are shown in Figure 10.

As expected, proton dissociation increases with increasing water content. At n = 1, approximately 40% dissociation was observed in the bare CNTs while in the fluorinated systems the percent dissociation was less than 20%. As mentioned earlier, each of the bare CNTs contain instances of sharing a proton between triflic acid/triflate molecules as well as interactions between water molecules, which was not observed in the fluorinated CNTs, which likely leads to the increased dissociation and the presence of Zundel cations. In 17N1, two different triflic acid molecules form direct hydrogen bonds with one triflate anion, each of which is typically in the bound state. This leads to dissociation of the proton originally associated with the triflate group forming a contact ion pair (CIP). These observations are also supported by the radial distribution function (RDF) between the triflic acid/triflate oxygen atoms and the protons shown in Figure 11a. The 17N1 RDF has the narrowest first peak of all the systems arising from the two bound protons but is followed by a clear minimum indicating less sharing of protons between triflic acid and water molecules. The first peak in the 14N1 RDF, on the other hand, is broader and occurs at a farther distance which is followed by a ridge revealing a greater tendency for sharing of protons both between triflic acid molecules and triflic acid and water molecules. In the fluorinated tubes, the first peak is shifted even farther but the distances between ~1.35-1.55 Å are less pronounced than in the bare systems suggesting that the protons are loosely bound but not fully dissociated with a much larger portion of the observed states as sharing between H_2O and CF_3SO_3H.

Increasing the hydration to n = 2 expectedly increased the degree of dissociation in all systems as well as the Zundel character of the dissociated protons. Surprisingly, ~86%

dissociation was observed in 14N2 with less than 1% bound states observed, while between 45 and 55% dissociation was observed in the other systems. At this hydration level the H_2O/CF_3SO_3H CN was the highest in 14N2 and was the only system in which this CN was higher than that between water molecules (Figure 2b) indicating that the water molecules and solvated protons have a greater propensity to hydrogen bond with multiple triflic acid molecules. As mentioned in the Introduction section that although electronic structure calculations on isolated PFSA fragments have revealed that proton dissociation may not occur at this low water content,[67, 68, 115] incorporation of multiple PFSA side chains enhances proton dissociation at low hydration levels through cooperative interactions between sulfonic acid groups and connectivity through a single water molecule.[42, 75-77, 79, 80] In each of the larger tubes, direct hydrogen bonding between triflic acid molecules lead to larger amounts of bound and shared CF_3SO_3H/CF_3SO_3H states. The dissociated proton(s), however, had greater separation from the triflic acid/triflate oxygen atoms than in 14N2 as shown in the RDF (Figure 11b) with very little instances of shared CF_3SO_3H/H_2O states. These states were quite frequent in 14F2, on the other hand, which exhibited the lowest dissociation but fewer bound states than in the larger tube. As mentioned earlier, the hydrogen bonding in this system exhibited somewhat selective solvation of one of the triflic acid molecules whose proton was generally in a dissociated state while the other acidic proton mostly rattled between triflic acid and water molecule oxygen atoms leading to a broader first peak in the RDF than in the larger systems again indicating that the protons are loosely bound but do not fully separate from the triflic acid groups. Further increasing the water content to n = 3 leads to near complete dissociation in all systems except the larger bare nanotube. Again, a hydrogen bond between triflic acid and triflate molecules led to a greater amount of bound and shared CF_3SO_3H/CF_3SO_3H states and decreases the overall proportion of dissociated protons. The average CN between water molecules and triflic acid oxygen atoms was the lowest and that between water molecules was the highest in 17N3 indicating a preference for interactions between water molecules. Indeed, hydrogen bonding from the water molecules to the oxygen atoms of the directly hydrogen bonded triflic acid/triflate molecules occurred but with average O···O and O···H distances of 2.81 and 1.87 Å, respectively, indicating weak hydrogen bonds as compared to that between water molecules which had respective distances of 2.61 and 1.58 Å. In fact, all

hydrogen bonds between triflic acid/triflate and water molecules here were relatively weak when compared to the other systems as indicated in the probability distribution of δ for all O–H···O_s hydrogen bonds between the triflate and water molecules shown in Figure 12 which contains no values of $\delta \geq$ -0.3 Å with a peak at approximately -0.8 Å. Note that since all protons are dissociated aside from the one involved in the direct hydrogen bond in 17N3 and very few observed instances of CF_3SO_3H/H_2O sharing in the other systems, the distribution shown always has water molecules/solvated protons as the hydrogen bond donor in the definition of δ. The dissociated protons in 17N3 were, thus, found have the greatest separation from the triflic acid oxygen atoms (which is also reflected in the RDF of Figure 11c) and over 80% of the time at least one proton was in the solvent-separated ion pair position donating hydrogen bonds to three water molecules resembling an Eigen cation. This was also found for one proton ~60% of the time in 14N3 but the system contained several single water molecules connecting two triflic acid molecules and the other dissociated protons remained more tightly bound as contact ion pairs. No complete separation of the protons from the triflate oxygen atoms was observed in either of the fluorinated CNTs.

OH···F hydrogen bonds

Finally, we examine potential interactions between the water molecules and solvated protons with the fluorine atoms. As mentioned in the Introduction section, AIMD simulations on model PFSA systems have reported evidence of weak water–fluorine interactions to some extent similar to hydrogen bonds, though longer. Although the nature of the interactions are not entirely clear, we examine them here as weak hydrogen bonds. While the geometric criteria for weak hydrogen bonds typically allows for a wide range of hydrogen bond angles,[116] the angular cutoff in the analysis was not relaxed from that used in the hydrogen bond analysis of triflic acid and water. The hydrogen bond distance cutoff, however, was taken as an H···F length less than 2.5 Å which is slightly longer than the second minimum of the H···O RDF in bulk water of ~2.46 Å.[117] It should be noted that changing the hydrogen bond criteria did not significantly impact the results. The hydrogen bond was required to exist for longer than 5 fs to be considered in the analysis to prevent transient motions of the water molecules from affecting the results. However, if the

hydrogen bond hopped between neighbouring fluorine atoms while maintaining the geometric criteria, it was still included in the determined number of O–H···F hydrogen bonds. In the bare CNTs, the only potential hydrogen bond accepting fluorine atoms come from the mobile CF_3SO_3H while in the fluorinated systems there are also the sites bound to the inner walls of the nanotube. No hydrogen bonding between a CF_3SO_3H sulfonic acid group and a fluorine atom was observed in any system, so the discussion is restricted to water molecules and solvated protons. The results for the fluorinated and bare systems are summarized in Tables 3 and 4, respectively, and Figure 13 shows the type of species involved in O–H···F hydrogen bonds. The O–H···F hydrogen bonding between water molecules and the triflic acid CF_3 groups had short lifetimes and were typically not found for multiple water molecules at any given time. In the fluorinated CNTs, these interactions were relatively rare with the most observed in 14F2 which occurred 9.2% of the time. This is likely due to the isolated water molecules and the orientation of one of the triflic acid groups (Figure 4b) leading to a lack of other available hydrogen bond acceptor sites. There was generally a greater propensity for O–H···F hydrogen bonding to the CF_3 groups in the bare CNT systems. No clear trend between the frequency of these interactions and the hydration level was found in the smaller bare tube, while in the larger system the amount of time they existed increased with hydration. One common feature observed is that all bare CNT systems that exhibited these interactions more than 15% of the time contained a direct hydrogen bond between triflic acid molecules which blocked available oxygen atoms from accepting hydrogen bonds (Figure S3). The percentage of time these O–H···F hydrogen bonds were observed in all systems is considerably higher than what was observed in our previous studies involving the CF_2 groups of CNTs functionalized with –CF_2SO_3H groups[84-86] suggesting that the additional mobility of the triflic acid groups in the present study may have an influence on these interactions.

Interactions between water and the fluorine atoms of the CNT wall were much more common than the fluorine atoms of triflic acid in the fluorinated systems, and the percent of the time at least one such O–H···F hydrogen bond existed increased as the hydration level increased with greater frequency in the smaller CNT. Representative snapshots of these interactions at all water contents are shown for the smaller and larger tubes in Figures S4 and S5, respectively. At n = 1, these were observed slightly over 60% of the time

in each system with the majority of the interactions expectedly coming from water molecules in the H_2O/CF_3SO_3H shared state as it was the most prevalent at this hydration level. The previously discussed hydrogen bond topography and isolation between water molecules at this low level of hydration generally leaves multiple OH bonds not involved in a hydrogen bond with a triflic acid $–SO_3H$ group (or other water molecules) leaving them open to interact with the fluorinated walls. The average H···F and O···F distances were approximately 2.24 and 3.13 Å in each case (which was approximately the same at all hydration levels) but the average lifetimes were found to be over twice as long in the smaller CNT. Nearly all occurrences of proton dissociation as a hydronium ion in 14F1 and the majority of those in 17F1 were accompanied by an O–H···F hydrogen bond indicating the fluorine atoms might provide a means to stabilize the excess charge. As the hydration level increases, the impact of the confinement dimensions on these interactions becomes more pronounced with at least one O–H···F bond occurring 91.5 and 99.1% of the time in the smaller CNT at n = 2 and 3, respectively, compared to 68.8 and 83.3% in the larger diameter tube. The majority of the observed Zundel states and over 60% of the H_3O^+ states in 14F2 were involved in hydrogen bond interactions with the fluorinated walls which is again likely due to the absence of neighbouring stabilizing hydrogen bond accepting oxygen sites from other water or triflic acid molecules. In 17F2, however, most of these interactions involved water molecules as the protonated cations, particularly H_3O^+, were typically found to hydrogen bond with other surrounding water or triflic acid molecules as indicated by the higher average total CN than 14F2 (Figure 2b). This was observed in both systems at n = 3 where more available hydrogen bond acceptor sites from water molecules promoted interactions that delocalized the excess charge over strong hydrogen bonds with neighbouring water molecules or triflate anions.

Conclusions

Single-walled CNTs of various diameter with different surface hydrophobicity were used as encapsulation vessels for mobile triflic acid groups at water contents of n = 1 – 3 H_2O/CF_3SO_3H to investigate proton dissociation and transfer at low water content in a confined environment. Each of the different systems exhibited distinctly different hydrogen bonding between water and triflic acid molecules. At the lowest hydration level, the H_2O in

the fluorinated CNTs were completely isolated from one another typically forming two hydrogen bonds with neighbouring CF_3SO_3H. This led to a propensity for the acidic protons to be shared between water and triflic acid molecules with dissociation occurring less than 20% of the time as a hydronium ion where, in each case, interactions with the fluorinated CNT walls appear to stabilize the hydrogen bond network. Direct hydrogen bonding between triflic acid molecules in the bare CNTs at n = 1 promoted interactions between water molecules and enhanced proton dissociation. Triflic acid hydrogen bond connectivity, both directly and through a single water molecule, had a continued effect on proton dissociation at higher hydration levels. This was most pronounced in 14N2 which had several single water molecules/solvated protons bridging two triflic acid molecules through hydrogen bonds and exhibited the highest proton dissociation at this hydration level. However, this also led to multiple protons being trapped between the triflate anions with less interaction between water molecules that promotes separation of the dissociated protons from the acid groups necessary for long-range proton transport. The greatest separation of dissociated protons was found in 17N3 but at the cost of a lower overall degree of dissociation due to direct hydrogen bonding between triflic acid/triflate molecules. This also led to strong interactions between water molecules which were able to form long chains that encompassed nearly all the water molecules in the system. These direct hydrogen bonds between the acid groups were observed at all hydration levels in the larger bare CNT resulting in the highest observed CNs between water molecules at each hydration level. This may be due to the additional free volume allowing for more orientational freedom for the mobile triflic acid molecules to form strong hydrogen bonds with a triflate anion upon dissociation to stabilize the charge. Weak hydrogen bonding between the water molecules and CF_3 groups was observed in all systems when open oxygen sites were not in the vicinity. This was particularly observed in the bare CNT systems that contained direct hydrogen bonds between the acid groups, which reduced the number of available hydrogen bond acceptor sites, and short-lived OH···F interactions appeared to provide some stabilization to the hydrogen bond network. Hydrogen bonding to the fluorinated walls (when present) occurred much more frequently than to the triflic acid fluorine atoms. In both systems, the frequency of these interactions increased with increasing hydration and to a greater extent in the smaller fluorinated CNT indicating an

influence of the confinement dimensions. Unlike our previous work,[84-86] the fluorine atoms did not appear to promote any particular state of the dissociated protons over those observed in the bare CNTs, aside from those at n = 1 where the isolated water molecules could not form Zundel cations. However, at n = 3, each of the bare CNT systems contained protons in the solvent-separated ion pair position surrounded by three water molecules as an Eigen cation. This was not observed in the fluorinated tubes due to the clustering of water molecules and the lack of mobility induced by the confinement dimensions and potential stabilization from the large number of OH···F interactions resulting in a fairly regular structure. It should be noted that the studies on hydrates of triflic acid[87, 88] revealed that inclusion of quantum nuclear effects through *ab initio* path integral techniques enhances the Zundel character. As these effects are absent in the present simulations, and the systems used are highly simplified models, the results presented here should not be taken as absolute values but as a relative comparison of how the confinement dimensions and surface hydrophobicity affect hydrogen bonding and proton dissociation.

Acknowledgement

JKC acknowledges support by the National Science Foundation under Grant No. DGE0801470, "Sustainable Technology through Advanced Interdisciplinary Research" (STAIR), awarded to the University of Tennessee, Knoxville. SJP acknowledges support by the DOE under contract number DE-FG36-07G017006. DOE support does not constitute an endorsement by DOE of the views expressed in this work. The primary simulations were made possible through use of the Kraken supercomputer at the National Institute for Computational Sciences, NICS, (http://www.nics.tennessee.edu). The authors also gratefully acknowledge: Dr. Luke Shulenburger at Sandia National Laboratory for performing the geometry optimizations using the hybrid, DFT-D3, and optB86b functionals, and Dr. Jun He at the University of Tennessee for performing the simulation using DFT-D2.

References

1. B. Smitha, S. Sridhar and A. A. Khan, *J. Membr. Sci.*, 2005, **259**, 10-26.
2. A. B. Stambouli and E. Traversa, *Renew. Sust. Energ. Rev.*, 2002, **6**, 295-304.
3. M. Granovskii, I. Dincer and M. A. Rosen, *Int. J. Hydrogen. Energ.*, 2006, **31**, 337-352.
4. K. D. Kreuer, S. J. Paddison, E. Spohr and M. Schuster, *Chem. Rev.*, 2004, **104**, 4637-4678.
5. O. Savadogo, *J. Power Sources*, 2004, **127**, 135-161.
6. M. A. Hickner, H. Ghassemi, Y. S. Kim, B. R. Einsla and J. E. McGrath, *Chem. Rev.*, 2004, **104**, 4587-4611.
7. Y. Y. Shao, G. P. Yin, Z. B. Wang and Y. Z. Gao, *J. Power Sources*, 2007, **167**, 235-242.
8. K. D. Kreuer, *ChemPhysChem*, 2002, **3**, 771-775.
9. K. D. Kreuer, *Solid State Ionics*, 1997, **97**, 1-15.
10. M. Ise, K. D. Kreuer and J. Maier, *Solid State Ionics*, 1999, **125**, 213-223.
11. K. D. Kreuer, *J. Membr. Sci.*, 2001, **185**, 29-39.
12. C. Yang, P. Costamagna, S. Srinivasan, J. Benziger and A. B. Bocarsly, *J. Power Sources*, 2001, **103**, 1-9.
13. L. Rubatat, A. L. Rollet, G. Gebel and O. Diat, *Macromolecules*, 2002, **35**, 4050-4055.
14. C. J. D. von Grotthuss, *Ann. Chim.*, 1806, **58**, 54-74.
15. M. Eikerling, A. A. Kornyshev, A. M. Kuznetsov, J. Ulstrup and S. Walbran, *J. Phys. Chem. B*, 2001, **105**, 3646-3662.
16. S. J. Paddison and R. Paul, *Phys. Chem. Chem. Phys.*, 2002, **4**, 1158-1163.
17. S. J. Paddison, R. Paul and K. D. Kreuer, *Phys. Chem. Chem. Phys.*, 2002, **4**, 1151-1157.
18. E. Spohr, P. Commer and A. A. Kornyshev, *J. Phys. Chem. B*, 2002, **106**, 10560-10569.
19. D. Marx, M. E. Tuckerman, J. Hutter and M. Parrinello, *Nature*, 1999, **397**, 601-604.
20. D. Marx, A. Chandra and M. E. Tuckerman, *Chem. Rev.*, 2010, **110**, 2174-2216.
21. N. Agmon, *Chem. Phys. Lett.*, 1995, **244**, 456-462.
22. M. E. Tuckerman, K. Laasonen, M. Sprik and M. Parrinello, *J. Phys. Chem.*, 1995, **99**, 5749-5752.
23. M. E. Tuckerman, K. Laasonen, M. Sprik and M. Parrinello, *J. Chem. Phys.*, 1995, **103**, 150-161.
24. H. Lapid, N. Agmon, M. K. Petersen and G. A. Voth, *J. Chem. Phys.*, 2005, **122**, 014506.
25. A. Chandra, M. E. Tuckerman and D. Marx, *Phys. Rev. Lett.*, 2007, **99**.
26. Z. Cao, Y. X. Peng, T. Y. Yan, S. Li, A. L. Li and G. A. Voth, *J. Am. Chem. Soc.*, 2010, **132**, 11395-11397.
27. J. C. Rasaiah, S. Garde and G. Hummer, *Annu. Rev. Phys. Chem.*, 2008, **59**, 713-740.
28. C. Dellago, M. M. Naor and G. Hummer, *Phys. Rev. Lett.*, 2003, **90**, 105902.
29. J. Kofinger, G. Hummer and C. Dellago, *Phys. Chem. Chem. Phys.*, 2011, **13**, 15403-15417.
30. J. Chen, X. Z. Li, Q. F. Zhang, A. Michaelides and E. G. Wang, *Phys. Chem. Chem. Phys.*, 2013, **15**, 6344-6349.
31. M. L. Brewer, U. W. Schmitt and G. A. Voth, *Biophys. J.*, 2001, **80**, 1691-1702.
32. S. J. Paddison, *Annu. Rev. Mater. Res.*, 2003, **33**, 289-319.
33. H. L. Lin, T. L. Yu, C. H. Huang and T. L. Lin, *J. Polym. Sci., Part B: Polym. Phys.*, 2005, **43**, 3044-3057.

34. C. H. Ma, T. L. Yu, H. L. Lin, Y. T. Huang, Y. L. Chen, U. S. Jeng, Y. H. Lai and Y. S. Sun, *Polymer*, 2009, **50**, 1764-1777.
35. G. Gebel and O. Diat, *Fuel Cells*, 2005, **5**, 261-276.
36. H. G. Haubold, T. Vad, H. Jungbluth and P. Hiller, *Electrochim. Acta*, 2001, **46**, 1559-1563.
37. W. Y. Hsu and T. D. Gierke, *J. Membr. Sci.*, 1983, **13**, 307-326.
38. K. A. Mauritz and R. B. Moore, *Chem. Rev.*, 2004, **104**, 4535-4585.
39. K. Schmidt-Rohr and Q. Chen, *Nature Mater.*, 2008, **7**, 75-83.
40. D.-S. Wu, S. J. Paddison and J. A. Elliott, *Energy Environ. Sci.*, 2008, **1**, 284-293.
41. G. Gebel, *Polymer*, 2000, **41**, 5829-5838.
42. J. A. Elliott and S. J. Paddison, *Phys. Chem. Chem. Phys.*, 2007, **9**, 2602-2618.
43. S. Yamamoto and S. A. Hyodo, *Polym. J.*, 2003, **35**, 519-527.
44. D. S. Wu, S. J. Paddison and J. A. Elliott, *Macromolecules*, 2009, **42**, 3358-3367.
45. D. S. Wu, S. J. Paddison, J. A. Elliott and S. J. Hamrock, *Langmuir*, 2010, **26**, 14308-14315.
46. A. Vishnyakov and A. V. Neimark, *J. Phys. Chem. B*, 2000, **104**, 4471-4478.
47. S. Urata, J. Irisawa, A. Takada, W. Shinoda, S. Tsuzuki and M. Mikami, *J. Phys. Chem. B*, 2005, **109**, 4269-4278.
48. S. S. Jang, V. Molinero, T. Cagin and W. A. Goddard, *J. Phys. Chem. B*, 2004, **108**, 3149-3157.
49. N. P. Blake, G. Mills and H. Metiu, *J. Phys. Chem. B*, 2007, **111**, 2490-2494.
50. I. H. Hristov, S. J. Paddison and R. Paul, *J. Phys. Chem. B*, 2008, **112**, 2937-2949.
51. T. J. F. Day, A. V. Soudackov, M. Cuma, U. W. Schmitt and G. A. Voth, *J. Chem. Phys.*, 2002, **117**, 5839-5849.
52. F. Wang and G. A. Voth, *J. Chem. Phys.*, 2005, **122**, 144105.
53. M. K. Petersen, F. Wang, N. P. Blake, H. Metiu and G. A. Voth, *J. Phys. Chem. B*, 2005, **109**, 3727-3730.
54. Y. J. Wu, H. N. Chen, F. Wang, F. Paesani and G. A. Voth, *J. Phys. Chem. B*, 2008, **112**, 467-482.
55. M. K. Petersen and G. A. Voth, *J. Phys. Chem. B*, 2006, **110**, 18594-18600.
56. E. Spohr, *Mol. Sim.*, 2004, **30**, 107-115.
57. P. Commer, C. Hartnig, D. Seeliger and E. Spohr, *Mol. Sim.*, 2004, **30**, 755-763.
58. D. Seeliger, C. Hartnig and E. Spohr, *Electrochim. Acta*, 2005, **50**, 4234-4240.
59. S. Dokmaisrijan and E. Spohr, *J. Mol. Liq.*, 2006, **129**, 92-100.
60. M. H. Eikerling and K. Malek, in *Modern Aspects of Electrochemistry, No 43*, ed. M. Schlesinger, 2009, DOI: 10.1007/978-0-387-49582-8_5, pp. 169-247.
61. S. J. Paddison, L. R. Pratt, T. Zawodzinski and D. W. Reagor, *Fluid Phase Equilib.*, 1998, **151**, 235-243.
62. S. J. Paddison and T. A. Zawodzinski Jr, *Solid State Ionics*, 1998, **113-115**, 333-340.
63. S. J. Paddison, L. R. Pratt and T. A. Zawodzinski, *J. New Mater. Electrochem. Sys.*, 1999, **2**, 183-188.
64. V. A. Glezakou, M. Dupuis and C. J. Mundy, *Phys. Chem. Chem. Phys.*, 2007, **9**, 5752-5760.
65. K. Sagarik, M. Phonyiem, C. Lao-Ngam and S. Chaiwongwattana, *Phys. Chem. Chem. Phys.*, 2008, **10**, 2098-2112.

66. M. Phonyiem, S. Chaiwongwattana, C. Lao-ngam and K. Sagarik, *Phys. Chem. Chem. Phys.*, 2011, **13**, 10923-10939.
67. C. Wang, J. K. Clark, M. Kumar and S. J. Paddison, *Solid State Ionics*, 2011, **199**, 6-13.
68. J. K. Clark, S. J. Paddison, M. Eikerling, M. Dupuis and T. A. Zawodzinski, *J. Phys. Chem. A*, 2012, **116**, 1801-1813.
69. M. Eikerling, S. J. Paddison and T. A. Zawodzinski, *J. New. Mat. Electr. Sys.*, 2002, **5**, 15-23.
70. S. J. Paddison, K. D. Kreuer and J. Maier, *Phys. Chem. Chem. Phys.*, 2006, **8**, 4530-4542.
71. C. Wang and S. J. Paddison, *Phys. Chem. Chem. Phys.*, 2010, **12**, 970-981.
72. L. Vilciauskas, S. J. Paddison and K. D. Kreuer, *J. Phys. Chem. A*, 2009, **113**, 9193-9201.
73. S. Urata, J. Irisawa, A. Takada, S. Tsuzuki, W. Shinoda and M. Mikami, *Phys. Chem. Chem. Phys.*, 2004, **6**, 3325-3332.
74. J. K. Clark II and S. J. Paddison, *Electrochim. Acta*, 2013, **101**, 279-292.
75. S. J. Paddison and J. A. Elliott, *J. Phys. Chem. A*, 2005, **109**, 7583-7593.
76. S. J. Paddison and J. A. Elliott, *Solid State Ionics*, 2006, **177**, 2385-2390.
77. S. J. Paddison and J. A. Elliott, *Phys. Chem. Chem. Phys.*, 2006, **8**, 2193-2203.
78. S. J. Paddison and J. A. Elliott, *Solid State Ionics*, 2007, **178**, 561-567.
79. J. K. Clark and S. J. Paddison, *Solid State Ionics*, 2012, **213**, 83-91.
80. J. K. Clark II, S. J. Paddison and S. J. Hamrock, *Phys. Chem. Chem. Phys.*, 2012, **14**, 16349-16359.
81. M. Eikerling, S. J. Paddison, L. R. Pratt and T. A. Zawodzinski, *Chem. Phys. Lett.*, 2003, **368**, 108-114.
82. Y. K. Choe, E. Tsuchida, T. Ikeshoji, S. Yamakawa and S. Hyodo, *J. Phys. Chem. B*, 2008, **112**, 11586-11594.
83. Y. K. Choe, E. Tsuchida, T. Ikeshoji, S. Yamakawa and S. Hyodo, *Phys. Chem. Chem. Phys.*, 2009, **11**, 3892-3899.
84. B. F. Habenicht, S. J. Paddison and M. E. Tuckerman, *Phys. Chem. Chem. Phys.*, 2010, **12**, 8728-8732.
85. B. F. Habenicht, S. J. Paddison and M. E. Tuckerman, *J. Mater. Chem.*, 2010, **20**, 6342-6351.
86. B. F. Habenicht and S. J. Paddison, *J. Phys. Chem. B*, 2011, **115**, 10826-10835.
87. R. L. Hayes, S. J. Paddison and M. E. Tuckerman, *J. Phys. Chem. B*, 2009, **113**, 16574-16589.
88. R. L. Hayes, S. J. Paddison and M. E. Tuckerman, *J. Phys. Chem. A*, 2011, **115**, 6112-6124.
89. A. Roudgar, S. P. Narasimachary and M. Eikerling, *J. Phys. Chem. B*, 2006, **110**, 20469-20477.
90. A. Roudgar, S. P. Narasimachary and M. Eikerling, *Chem. Phys. Lett.*, 2008, **457**, 337-341.
91. S. R. Narasimachary, A. Roudgar and M. Eikerling, *Electrochim. Acta*, 2008, **53**, 6920-6927.
92. M. A. Ilhan and E. Spohr, *J. Phys.: Condens. Matter*, 2011, **23**, 234104.
93. M. Falk, *Canad. J. Chem.*, 1980, **58**, 1495-1501.
94. R. Basnayake, G. R. Peterson, D. J. Casadonte and C. Korzeniewski, *J. Phys. Chem. B*, 2006, **110**, 23938-23943.

95. D. E. Moilanen, I. R. Piletic and M. D. Fayer, *J. Phys. Chem. A*, 2006, **110**, 9084-9088.
96. G. Kresse and J. Hafner, *Phys. Rev. B*, 1993, **47**, 558-561.
97. G. Kresse and J. Hafner, *Phys. Rev. B*, 1994, **49**, 14251-14269.
98. G. Kresse and J. Furthmuller, *Phys. Rev. B*, 1996, **54**, 11169-11186.
99. G. Kresse and J. Furthmuller, *Comput. Mater. Sci.*, 1996, **6**, 15-50.
100. P. E. Blochl, *Phys. Rev. B*, 1994, **50**, 17953-17979.
101. G. Kresse and D. Joubert, *Phys. Rev. B*, 1999, **59**, 1758-1775.
102. J. P. Perdew, K. Burke and M. Ernzerhof, *Phys. Rev. Lett.*, 1996, **77**, 3865-3868.
103. J. P. Perdew, K. Burke and M. Ernzerhof, *Phys. Rev. Lett.*, 1997, **78**, 1396-1396.
104. C. Adamo and V. Barone, *J. Chem. Phys.*, 1999, **110**, 6158-6170.
105. L. Schimka, J. Harl and G. Kresse, *J. Chem. Phys.*, 2011, **134**, 024116.
106. S. Grimme, J. Antony, S. Ehrlich and H. Krieg, *The Journal of Chemical Physics*, 2010, **132**, 154104.
107. J. Klimes, D. R. Bowler and A. Michaelides, *J. Phys. Condens. Matter.*, 2010, **22**, 022201.
108. J. Klimes, D. R. Bowler and A. Michaelides, *Phys. Rev. B*, 2011, **83**, 195131.
109. S. Grimme, *J. Comput. Chem.*, 2006, **27**, 1787-1799.
110. D. Laage and J. T. Hynes, *Science*, 2006, **311**, 832-835.
111. R. Kumar, J. R. Schmidt and J. L. Skinner, *J. Chem. Phys.*, 2007, **126**, 204107.
112. B. C. Wood and N. Marzari, *Phys. Rev. B*, 2007, **76**, 134301.
113. L. Vilciauskas, M. E. Tuckerman, G. Bester, S. J. Paddison and K. D. Kreuer, *Nature Chemistry*, 2012, **4**, 461-466.
114. A. Hassanali, F. Giberti, J. Cuny, T. D. Kuhne and M. Parrinello, *Proc. Nat. Acad. Sci. USA*, 2013, **110**, 13723-13728.
115. S. J. Paddison, *J. New. Mat. Electr. Sys.*, 2001, **4**, 197-207.
116. T. Steiner, *Angew. Chem. Int. Ed.*, 2002, **41**, 48-76.
117. A. K. Soper, *ISRN Physical Chemistry*, 2013, **2013**, 279463.

Table 1. System parameters

System	Diameter (Å)†	Length (Å)	# H_2O	# CF_3SO_3H
14N1	11.3	13.1	3	3
14N2	11.6	13.5	6	3
14N3	11.0	17.1	9	3
14F1	11.6 (8.9)	13.5	2	2
14F2	11.1 (8.4)	17.3	4	2
14F3	11.4 (8.7)	17.8	6	2
17N1	13.3	12.8	4	4
17N2	13.9	13.3	8	4
17N3	13.3	12.8	9	3
17F1	13.9 (11.2)	13.3	3	3
17F2	13.2 (10.5)	12.7	4	2
17F3	13.3 (10.6)	12.8	6	2

†Based on the CNT carbon atoms, numbers in parentheses subtract C–F bond lengths.

Table 2. Averaged connectivity data.†

System	# Chains	# Chains per CF_3SO_3H	# H_2O Oxygen Atoms	# CF_3SO_3H Oxygen Atoms	# Rings
14N1	1.98 (1.98)	0.66 (0.66)	1.36 (1.36)	1.82 (1.82)	0.0012
14N2	1.73 (1.73)	0.58 (0.58)	3.38 (3.38)	2.37 (1.82)	0.0039
14N3	1.72 (1.63)	0.57 (0.54)	4.51 (3.41)	2.63 (2.33)	0.53
14F1	1.89 (1.89)	0.94 (0.94)	1.00 (1.00)	2.00 (2.00)	-
14F2	2.00 (2.00)	1.00 (1.00)	2.00 (2.00)	1.80 (1.80)	-
14F3	2.00 (2.00)	1.00 (1.00)	2.90 (2.90)	1.95 (1.95)	0.0030
17N1	1.94 (1.94)	0.48 (0.48)	1.80 (1.80)	1.96 (1.96)	0.0026
17N2	1.32 (1.27)	0.33 (0.32)	5.53 (4.98)	2.63 (2.41)	0.29
17N3	1.23 (1.08)	0.41 (0.36)	6.45 (5.80)	2.42 (2.20)	0.33
17F1	2.91 (2.91)	0.97 (0.97)	1.00 (1.00)	2.02 (2.02)	-
17F2	1.00 (0.74)	0.50 (0.37)	3.89 (3.86)	1.85 (1.80)	0.26
17F3	1.08 (1.03)	0.54 (0.51)	5.15 (4.59)	3.06 (2.75)	0.26

†Numbers in parentheses represent values when ring connections are removed.

Table 3. O–H···F hydrogen bond data for the fluorinated systems.

System	% Time O–H···F (CNT) Exists	Average O–H···F (CNT) Life (fs)	% Time O–H···F (Triflic) Exists	Average O–H···F (Triflic) Life (fs)
14F1	64.1	127.2	2.9	21.2
14F2	91.5	54.0	9.2	35.4
14F3	99.2	137.1	3.9	27.0
17F1	63.4	58.2	0.73	20.3
17F2	68.8	70.4	4.1	22.4
17F3	83.3	116.9	6.3	36.7

Table 4. O–H···F hydrogen bond data for the bare systems.

System	% Time O–H···F (Triflic) Exists	Avg. O–H···F (Triflic) Life (fs)
14N1	29.3	53.1
14N2	7.2	26.7
14N3	14.7	31.0
17N1	16.9	41.5
17N2	18.2	40.6
17N3	25.5	36.8

Figure Captions

Figure 1. Systems used in the present study shown for n = 3: (a) 14N3, (b) 14F3, (c) 17N3, and (d) 17F3. The different coloured spheres represent different atom types where: grey–carbon, red–oxygen, white–hydrogen, yellow–fluorine, and orange–sulphur.

Figure 2. Coordination numbers of the water molecules defined by the average number of donated and accepted water/water and water/triflic acid sulfonate group hydrogen bonds for each system for: (a) n = 1, (b) n = 2, and (c) n = 3.

Figure 3. Representative snapshots of the hydrogen bond network for n = 1 for: (a) 14N1, (b) 14F1, (c) 17N1, and (d) 17F1. Hydrogen bonds are denoted by dashed lines. A portion of periodic images have been included represented by coloured rods to show the local environment. The CNT walls have been omitted for clarity.

Figure 4. Representative snapshots of the hydrogen bond network for n = 2 for: (a) 14N2, (b) 14F2, (c) 17N2, and (d) 17F2. Hydrogen bonds are denoted by dashed lines. A portion of periodic images have been included represented by coloured rods to show the local environment. The CNT walls have been omitted for clarity.

Figure 5. Representative snapshots of the hydrogen bond network for n = 3 for: (a) 14N3, (b) 14F3, (c) 17N3, and (d) 17F3. Hydrogen bonds are denoted by dashed lines. A portion of periodic images have been included represented by coloured rods to show the local environment. The CNT walls have been omitted for clarity.

Figure 6. The average number of chains per CF_3SO_3H for all CNT/triflic acid+H_2O systems: (a) including oxygen atoms that are part of rings and (b) omitting oxygen atoms involved in ring connections.

Figure 7. Average chain lengths defined by the number of oxygen atoms involved in all systems partitioned into oxygen atoms of H_2O and CF_3SO_3H: (a) with and (b) without

oxygen atoms involved in ring connections. (c) and (d) show the average fraction of total oxygen atoms in the system involved per chain.

Figure 8. The data for rings showing (a) the average number of rings and (b) the average length of rings partitioned into H_2O and CF_3SO_3H oxygen atoms.

Figure 9. Snapshot down the CNT axis in 17F3 showing the water molecules in a structured domain away from the triflic acid CF_3 head groups.

Figure 10. State of the protons in each system by hydration level: (a) n = 1, (b) n = 2, and (c) n = 3. See text for definition of different states.

Figure 11. Radial distribution functions between the oxygen atoms of triflic acid sulfonate groups, O_S, and hydrogen atoms by hydration level: (a) n = 1, (b) n = 2, and, (c) n = 3.

Figure 12. Probability distribution of the asymmetric stretch coordinate, $\delta = R_{O_aH} - R_{O_dH}$, for all hydrogen bonds between water molecules and triflic acid SO_3H groups for each system at n = 3. In all cases at this hydration level, water molecules/solvated protons act as the hydrogen bond donor.

Figure 13. Percent time at least one OH···F hydrogen bond exists between the water molecules and/or solvated protons and (a) the fluorinated CNT walls and (b) the fluorine atoms of the mobile triflic acid groups partitioned into the types of species involved.

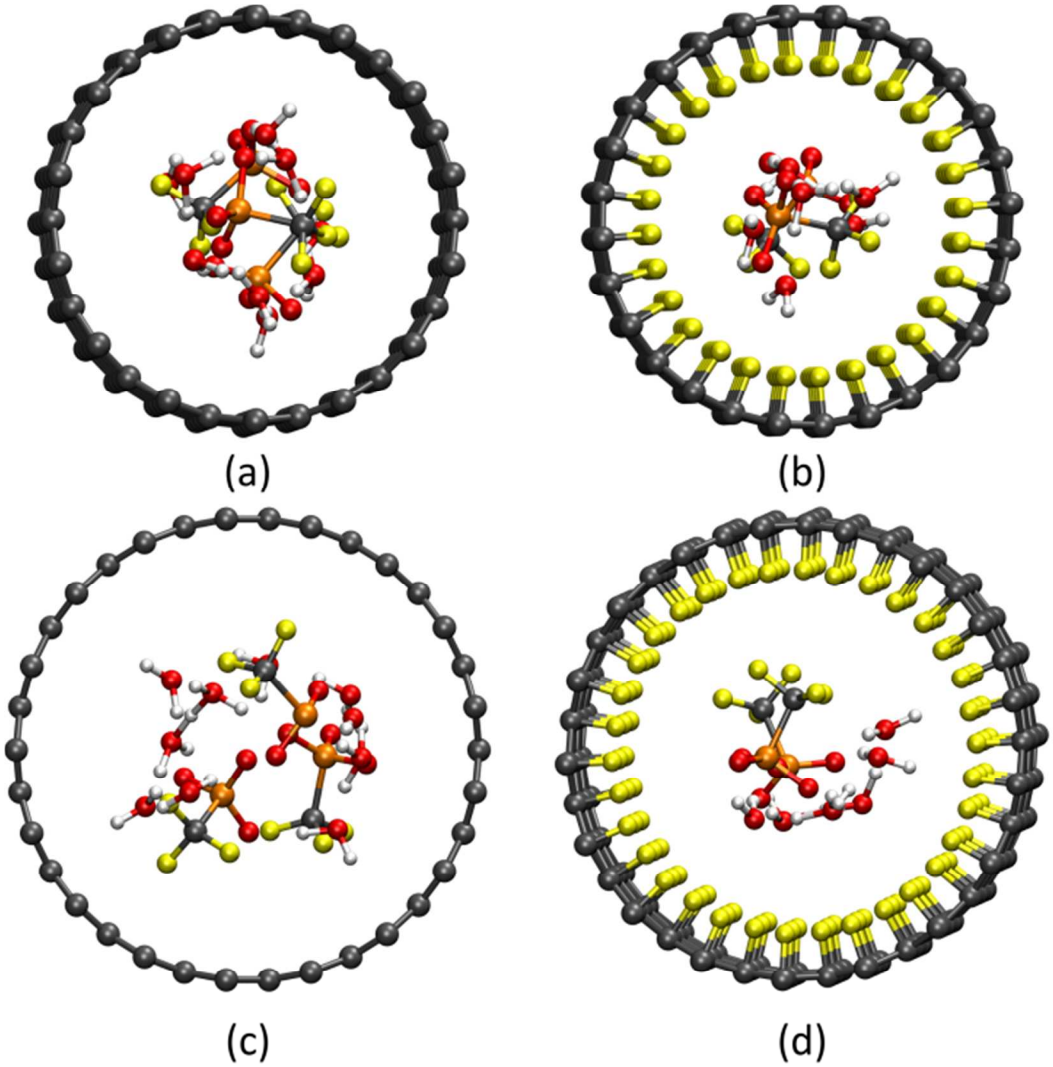

Fig. 1

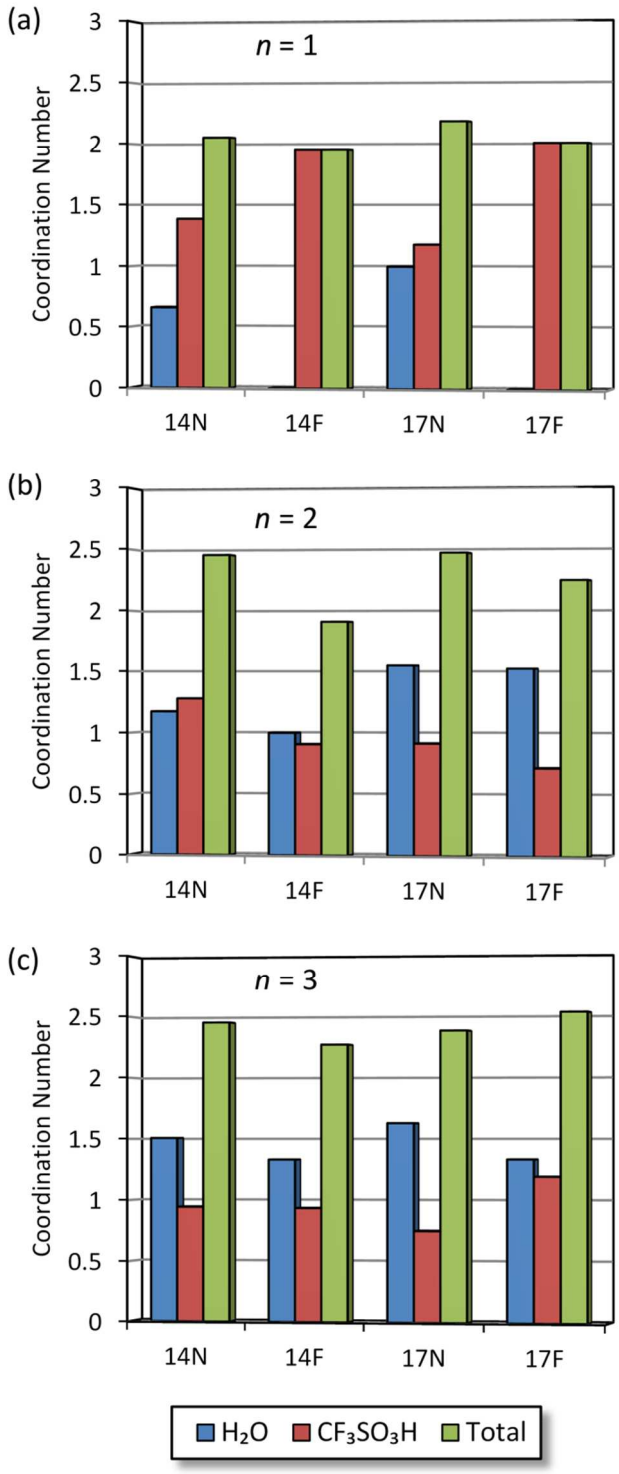

Fig. 2

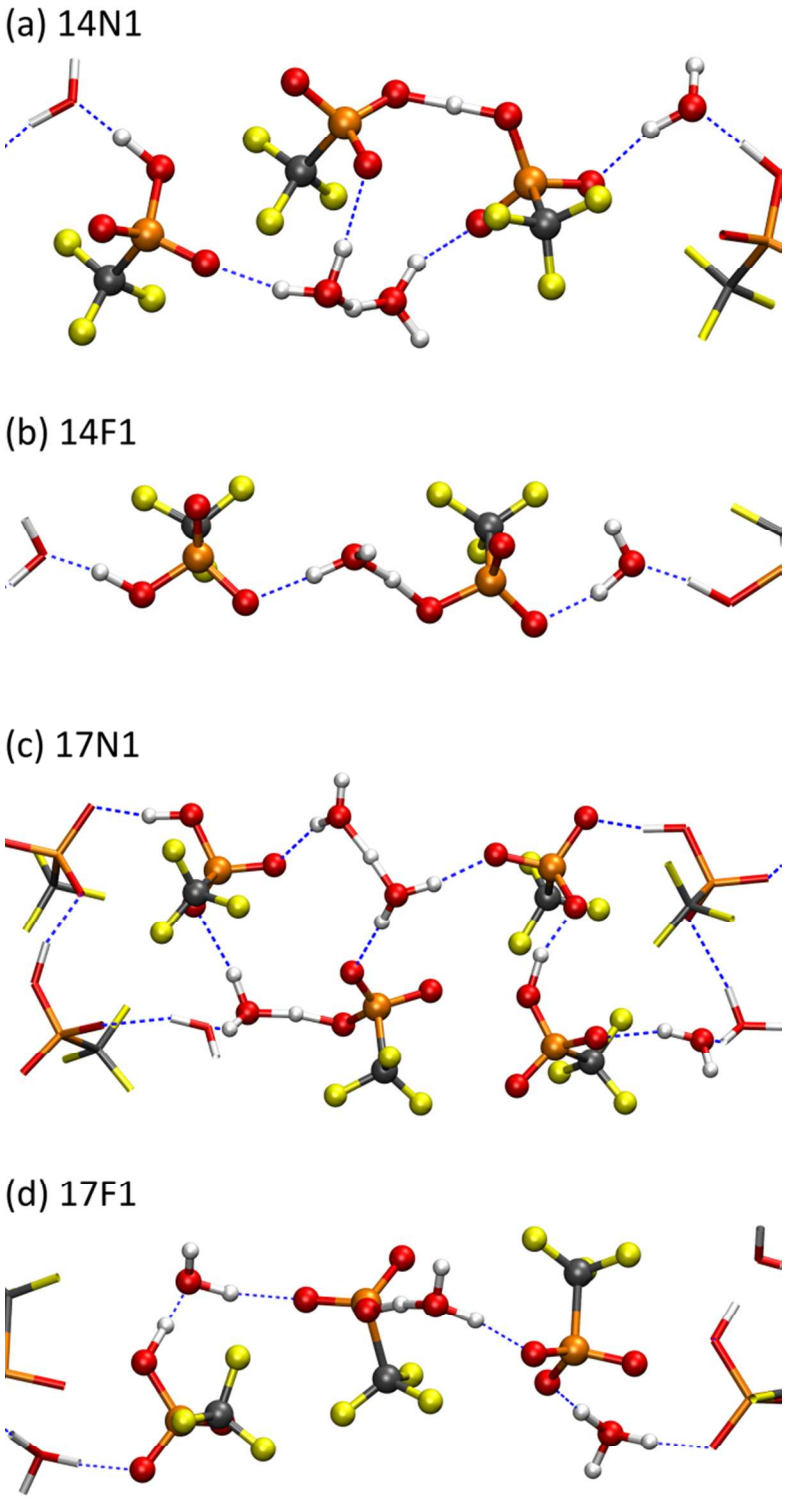

Fig. 3

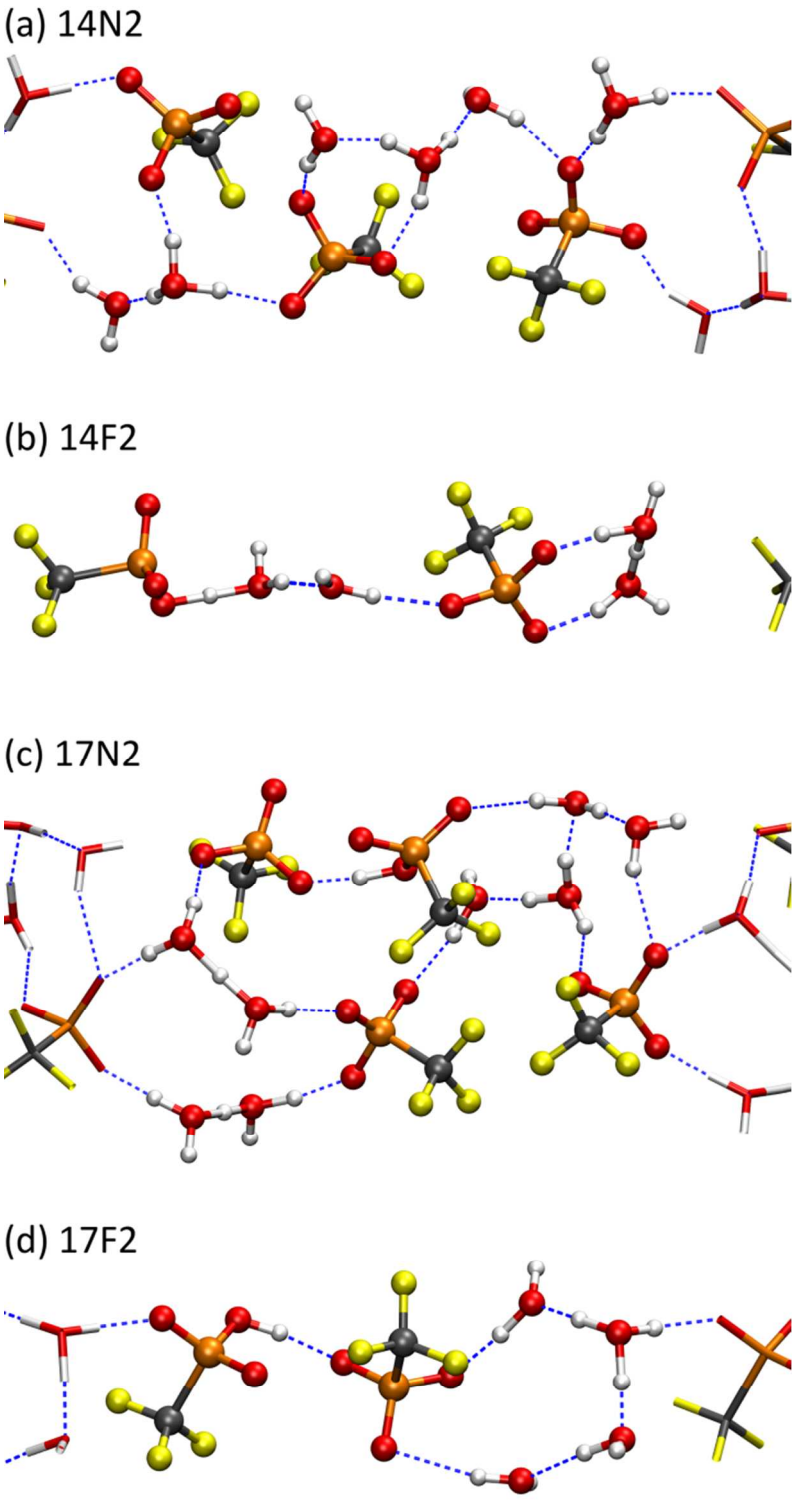

Fig. 4

(a) 14N3

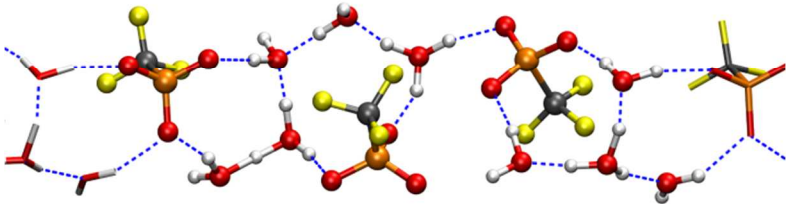

(b) 14F3

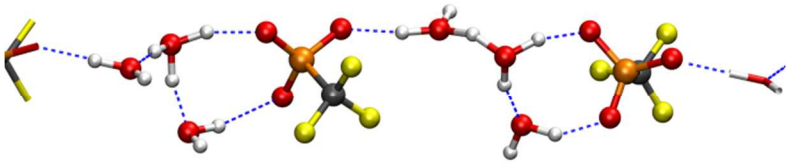

(c) 17N3

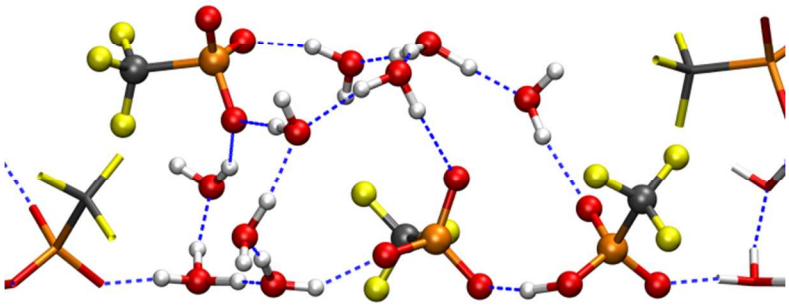

(d) 17F3

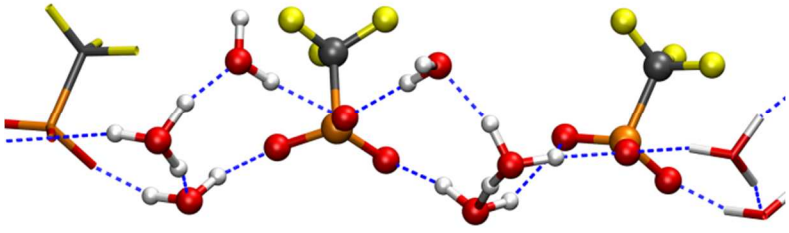

Fig. 5

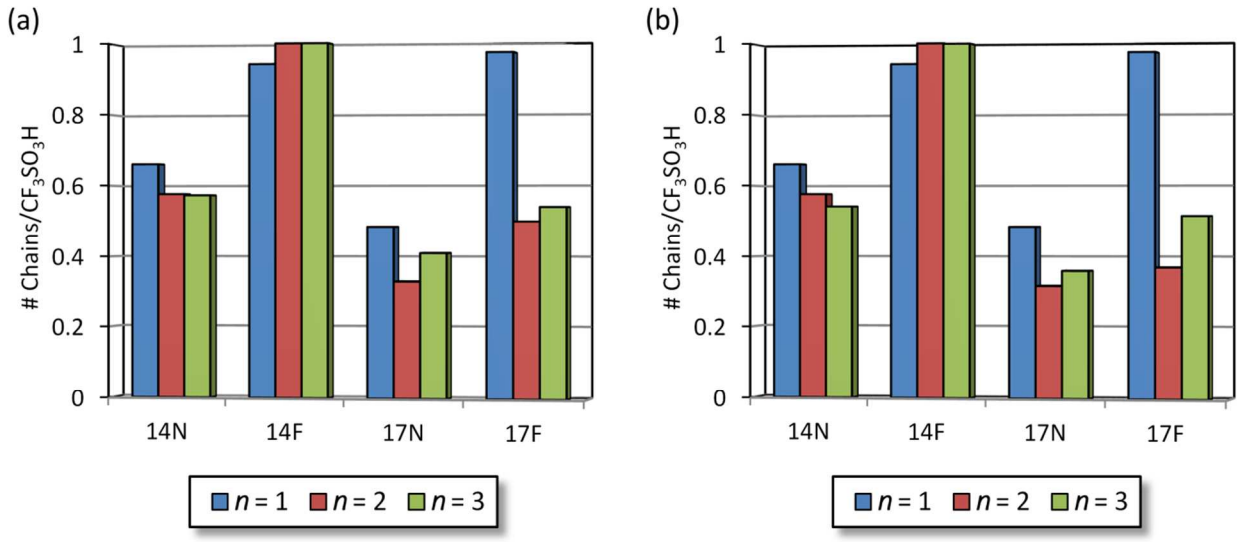

Fig. 6

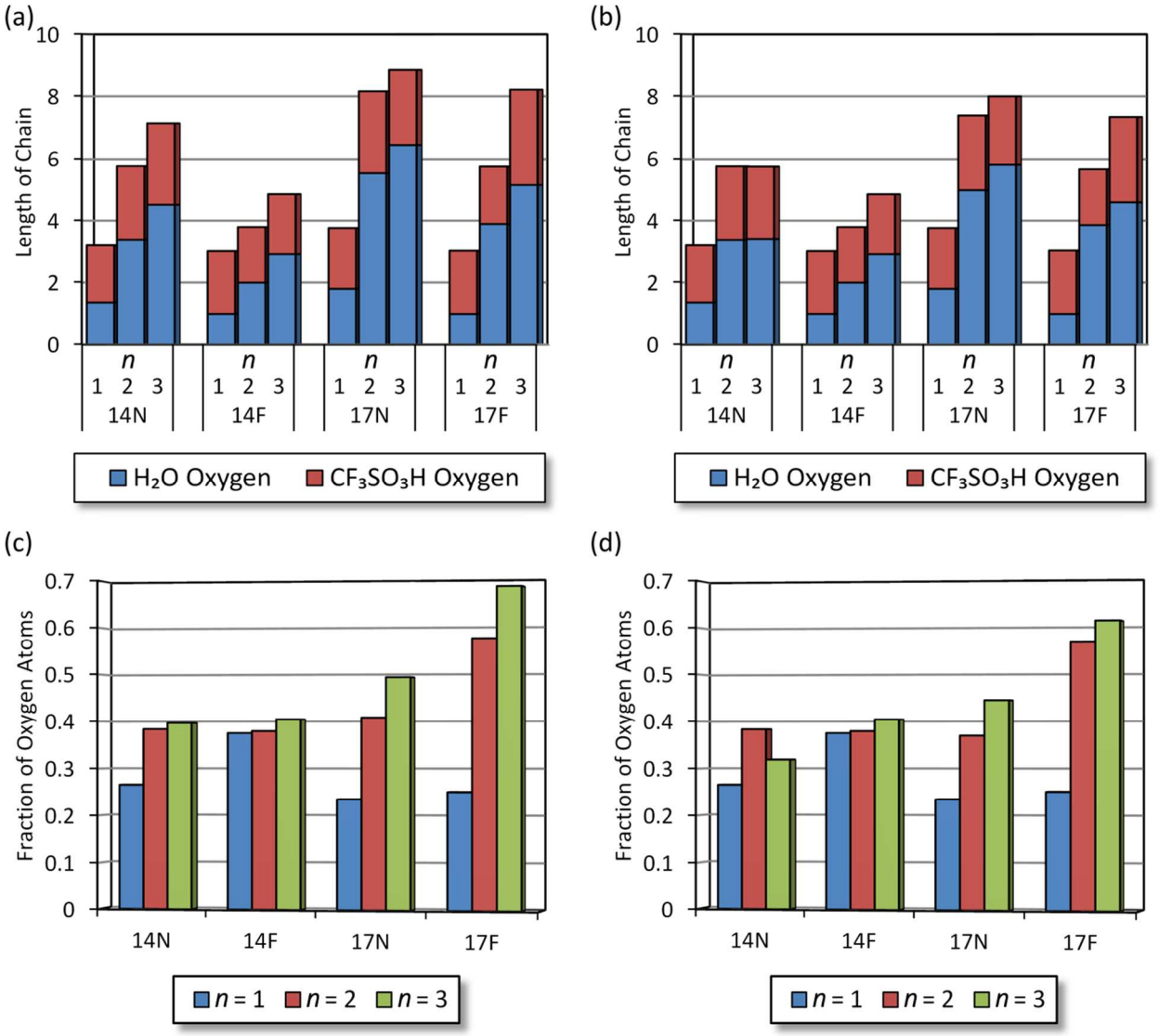

Fig. 7

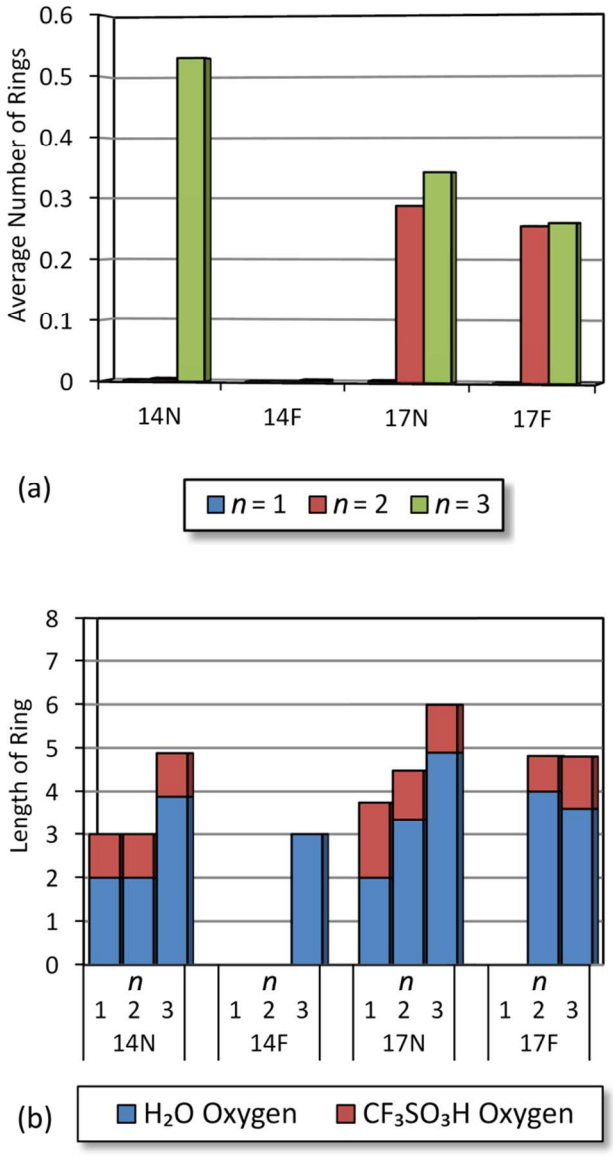

Fig. 8

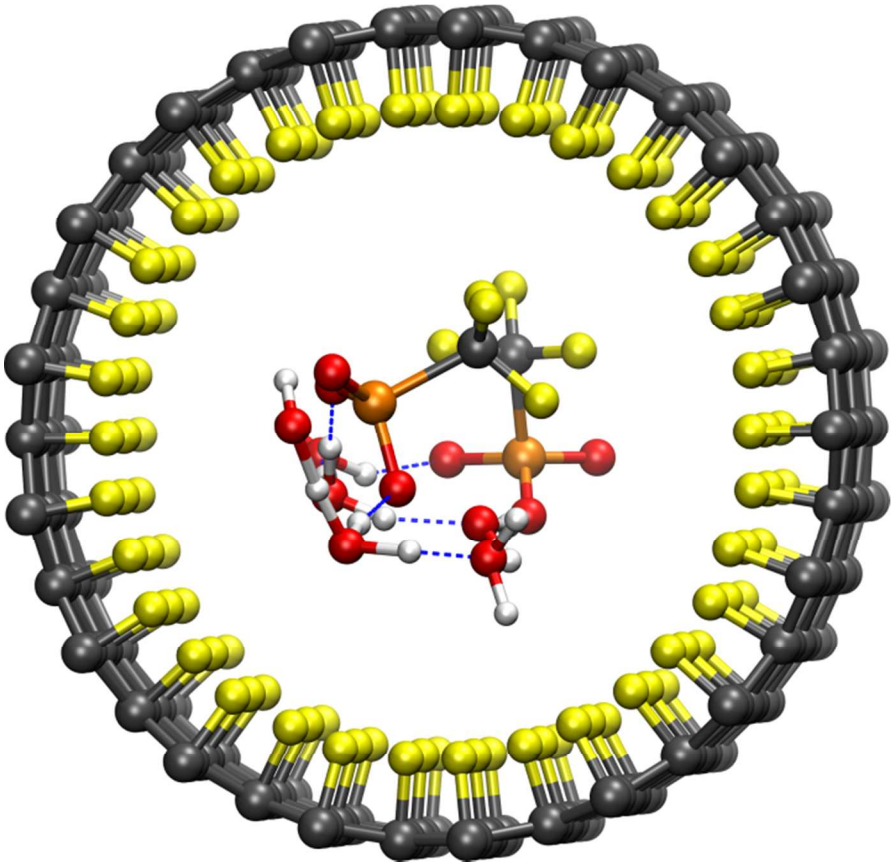

Fig. 9

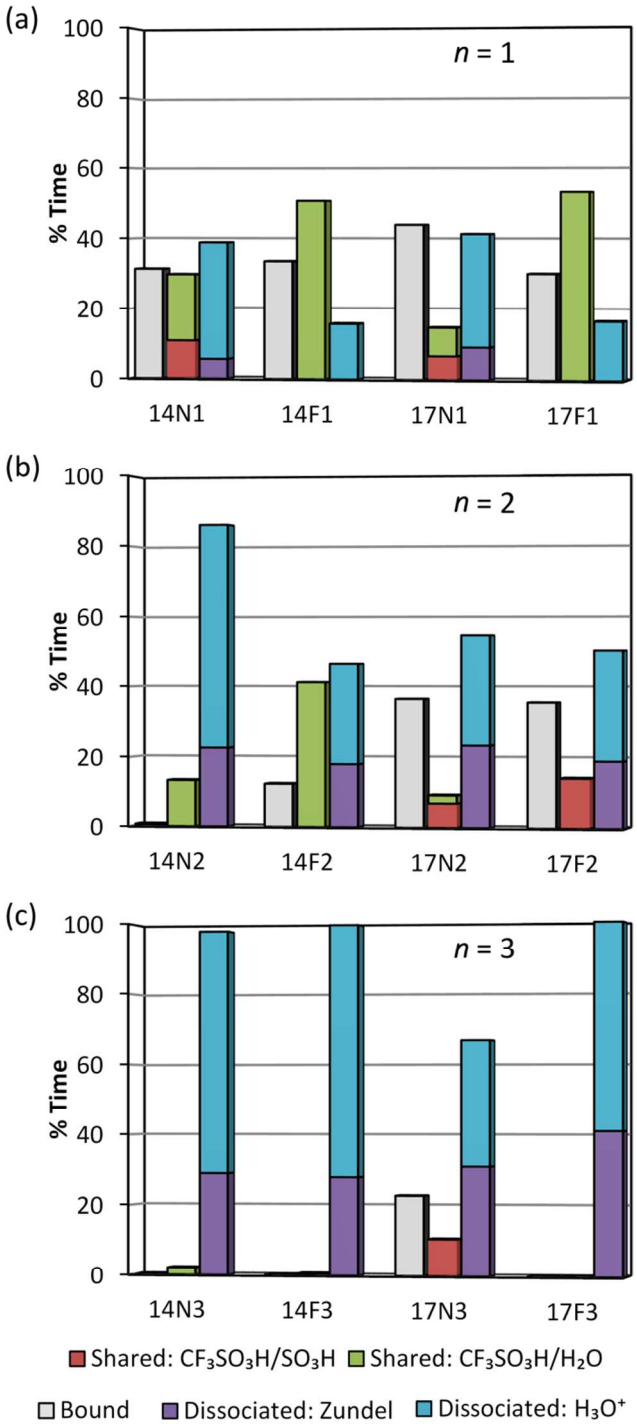

Fig. 10

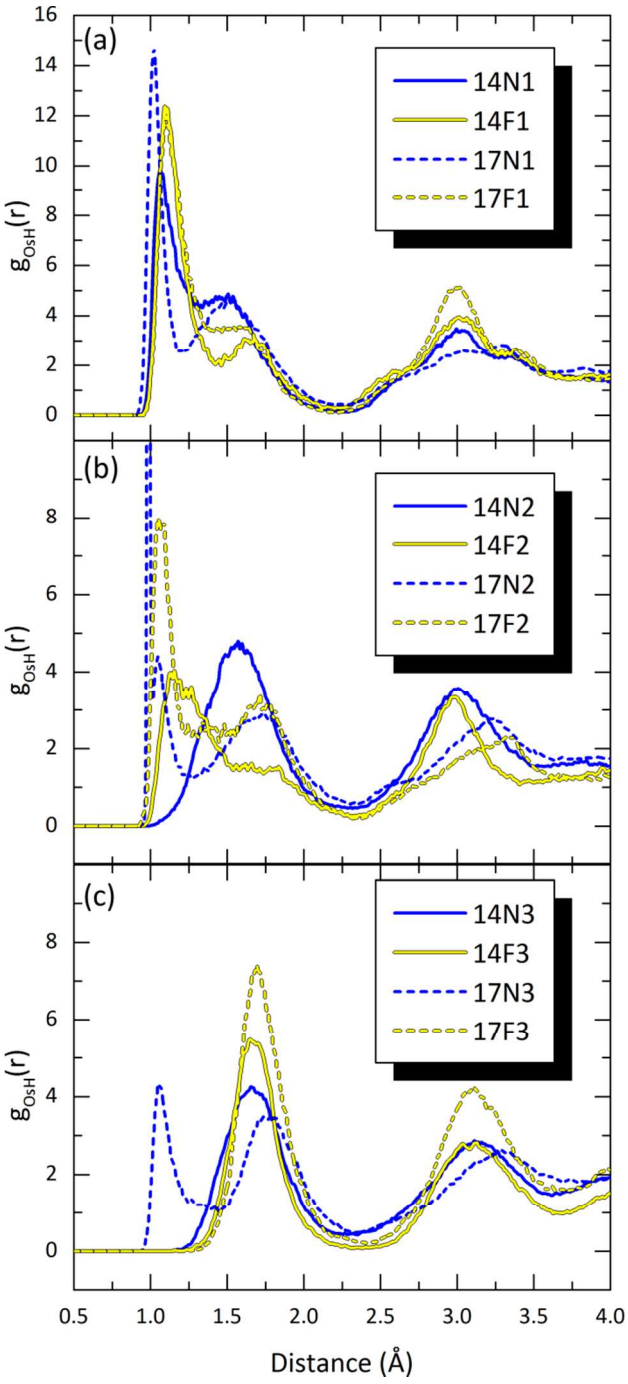

Fig. 11

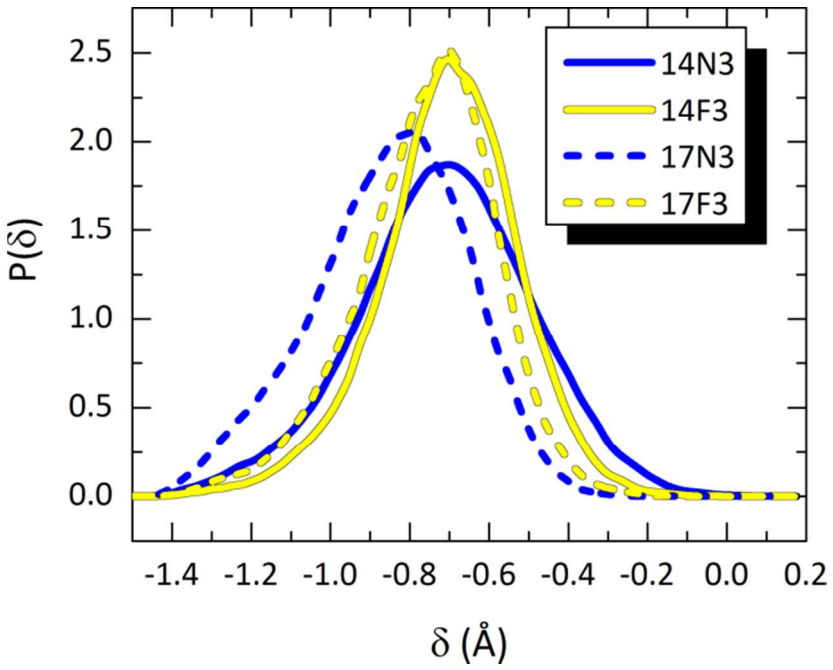

Fig. 12

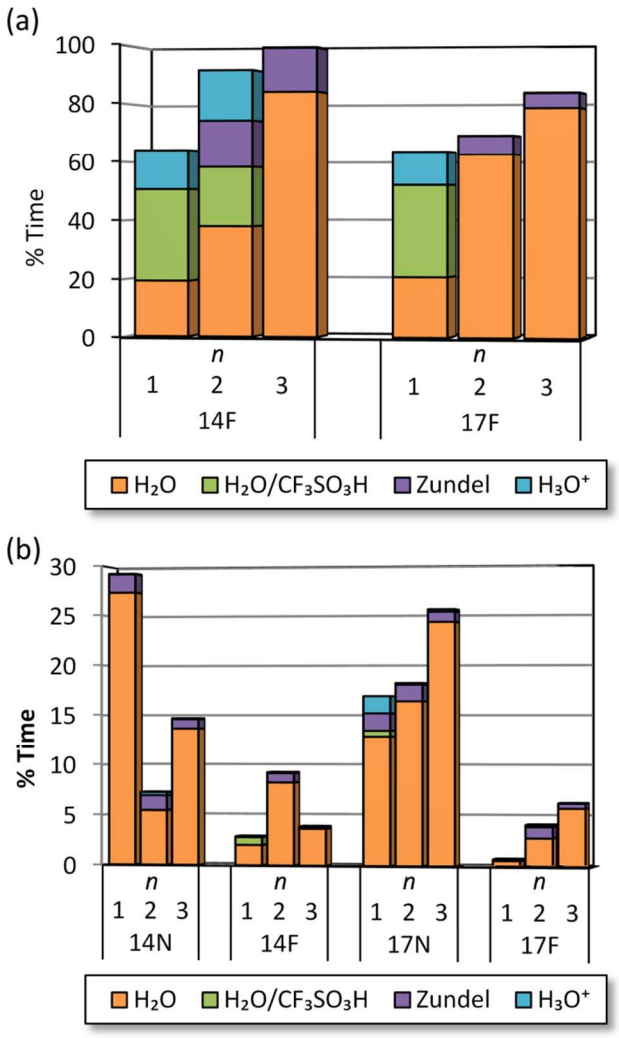

Fig. 13